PCCP

Accepted Manuscript

ROYAL SOCIETY OF CHEMISTRY

www.rsc.org/pccp

Combined NMR and Molecular Dynamics Modeling Study of Transport Properties in Sulfonamide Based Deep Eutectic Lithium Electrolytes in LiTFSI Based Binary Systems

Allen D. Pauric[1], Ion C. Halalay[2], and Gillian R. Goward[1]*

[1]Department of Chemistry, McMaster University, Hamilton, Canada.

[2]General Motors R&D Center, Warren, MI, USA.

ABSTRACT

The trend toward Li-ion batteries operating at increased (> 4.5 V vs. Li/Li^+) voltages requires the development of novel classes of lithium electrolytes with electrochemical stability windows exceeding those of $LiPF_6$/carbonate electrolyte solutions. Several new classes of electrolytes have been synthesized and investigated over the past decade in the search for LIB electrolytes with improved properties (increased hydrolytic stability, improved thermal abuse tolerance, higher oxidation voltages, etc.) compared with the present state-of-the-art $LiPF_6$ and organic carbonates-based formulations. Among these are deep eutectic electrolytes (DEEs), which share many beneficial characteristics with ionic liquids, such as low vapor pressure and large electrochemical stability windows, with the added advantage of a significantly higher lithium transference number. The present work presents the pulsed field gradient NMR characterization of the transport properties (diffusion coefficients and cation transport numbers) of binary DEEs consisting of a sulfonamide solvent and lithium bis(trifluoromethanesulfonyl)imide salt. Insights into the structural and dynamical properties, which enable one to rationalize the observed ionic conductivity behavior were obtained from a combination of NMR data and MD simulations. The insights thus gained should assist the formulation of novel DEEs with improved properties for LIB applications.

*Corresponding author; e-mail: goward@mcmaster.ca

1. Introduction

The electrochemical and transport properties of $LiPF_6$ and organic carbonate-based electrolytes have enabled the proliferation of lithium ion batteries (LIBs) in applications ranging from portable consumer electronics to electrified vehicles. However, their thermal abuse tolerance behavior is less than optimal, at least in some practical applications (portable consumer electronics and computers). In addition, while their electrochemical window is sufficient for present day electrode chemistries, the trend toward the use of positive electrode materials with higher operation voltages (in excess of 4.3 and preferably 5.0 V vs. L/Li^+) requires electrolyte solutions with greater electrochemical stability. In order to address these concerns, alternative electrolytes have been proposed and investigated over the past ten to fifteen years.

One of the most prominent classes of alternative electrolytes are ionic liquids (ILs) [1]. An ionic liquid is a molten salt (thus comprised solely of a cations and anions mixture) with a close-to-ambient (<40 ºC) melting temperature. The keen interest in ILs stems from a number of properties advantageous for various battery applications. Pertinent to the context of LIBs are exceptionally low vapor pressures (often in the nano-Torr range), leading to negligible flammability [2], and very wide electrochemical stability windows [3]. Unfortunately, these very desirable properties are often accompanied by a very high viscosity and low mobility of the Li^+ cation, which is a potential showstopper for automotive LIB applications. Even more challenging, however, is the temperature dependence of the transport properties of ILs. The introduction of a lithium salt into an ionic liquid often results in a very low transference number, typically less than 0.2 as a consequence of Li^+ not being the sole cation present in the electrolyte solution. Furthermore, the migration and accumulation of positive ions other than Li^+ cations near the electrode surfaces produces a concentration gradient which opposes the direction of Li^+ migration and diffusion, [4] thus leading to a serious impairment of the rate performance of most LIBs containing IL-based electrolyte solutions.

Deep eutectic electrolytes (DEEs), sometimes also called deep eutectic solvents (or DESs [5]) have been investigated as alternative electrolytes which may avoid the issue of the low lithium transference number that plagues LIB electrolytes with an IL as a major

component. The primary difference between DEEs and ILs is that, whereas ILs are composed solely of cations and anions, DEEs are mixtures of a charge-delocalized organic salt with a small polar organic molecule. Such an arrangement disrupts the ionic bonding of the salt and also weakens any strong molecular interactions (e.g., hydrogen bonding) present in the polar organic solvent. Note that in their pure states, all components of a DEE are solids. Upon homogenization in appropriate proportions, a DEE will display a melting point depression which can be more than 100 ºC below the lowest melting point of either pure component. A prominent and well-studied example of a binary DEE is composed of urea and choline chloride [6–8]. Note that, while DEEs display transport and electrochemical properties similar to those of other concentrated electrolyte solutions based on solutions of lithium salts in low vapor pressure solvents such as propylene carbonate, dimethyl sulfoxide, sulfones, or glymes (see, e.g. [9]), the essential distinction of DEEs is that both the solvents and salts entering their composition are solids at above-ambient temperatures, in their pure states.

Many of the properties inherent in ILs are also present in DEEs, including an extremely low vapor pressure (hence minimal flammability) and a wide electrochemical stability window (reaching 5.5 V vs. Li/Li^+ in some cases). The distinct advantage of DEEs over ILs for LIB applications is the presence of a single cation, namely Li^+. ILs typically require a relatively high concentration of dissolved lithium salt in order to be useful for LIBs. This leads to the presence of at least three separate ionic species, a common anion and two different cations. The presence of the additional cation causes a significant reduction of the Li^+ transference number in ILs; values lower than 0.15 are not uncommon. The importance of the Li^+ transference number is often overlooked in the literature on ILs. Note that a specific conductivity increased at the expense of a considerably reduced Li^+ transference number to values in the 0.05 to 0.15 range [10] is of no relevance for LIBs used in automotive applications; which, e.g., generally require charge/discharge rates of at least C/3. In commonly used liquid organic electrolyte solutions, transference numbers do not exhibit much variation, having mostly values in the 0.25 to 0.45 range [11]. However, DEEs can display significantly higher transport numbers (reaching 0.7 for some discussed here) and may therefore demonstrate acceptable cycling performance in full cells even at specific conductivity values lower than those typical for LIB industry state-of-the-art $LiPF_6$ in organic carbonates electrolyte solutions. (Note: While transference numbers and transport numbers

do not have the same physical meaning, they typically agree within a few (2 to 5) percent and so their “mixed comparison” is legitimate for the purpose of an approximate comparison, as is the case for the present discussion. See the Appendix for further justification why transport numbers can act as surrogates for transference numbers in the present case, for a limited number of DEEs of interest, i.e., those with the highest specific conductivity values from the present study.) In addition to the advantage of increased transference numbers, even when compared with liquid electrolytes, DEEs are less expensive to produce than ILs, due to the considerably greater ease in the manufacture of simple organic molecules. They do, however, suffer from some of the drawbacks of ionic liquids. These include a high viscosity and a specific conductivity significantly lower than liquid organic electrolyte solutions, particularly at low temperatures. Of particular interest for LIBs are DEEs comprised of a mixture of an organic lithium salt such as lithium bis(trifluoromethanesulfonyl)imide (LiTFSI) and a solvent consisting of small, polar, organic molecules [12-15].

Note that most DEEs contain organic molecules with the propensity for hydrogen bonding. This has traditionally been considered detrimental to LIBs performance, although recent work suggests otherwise [16]. Hydrogen bonds in the organic solvent component are important for deep eutectics formation because they can be broken through the introduction of an organic salt. In this context, it should be noted that hydrogen bonds can be represented by a strong permanent dipole. Any molecular organic solid with molecules that participate in strong dipolar interactions should, in principle, be suitable for use in a DEE. When considering a solution state system, the term “Coulombic interaction” [17] refers to the electrostatic forces between two ions. For both polar and non-polar molecules, the sum of their interactions are described by their van der Waals interactions [18]. The strongest of these are interactions between permanent dipoles, followed by those between induced dipoles and permanent dipoles, and finally by the interaction between two instantaneous (induced) dipoles. A practically useful deep eutectic would minimize the sum of all these forces to the greatest extent possible. This would result in the least resistance to diffusion and thus very likely translate into an increased Li^+ conductivity.

While the number of DEE studies reported in the literature is increasing [19], there exists a need for research addressing fundamental properties, including solution state structure and transport properties, to guide the search for DEEs with improved properties for

various applications, including Li-ion batteries. To this end, the present study is concerned with LiTFSI-based binary deep eutectic electrolytes based on lithium fluorinated imide salts and a sulfonamide organic component. A specific emphasis is placed on experimental measurements of the individual diffusion coefficients for the anion, cation, and organic components through pulsed field gradient nuclear magnetic resonance (PFG-NMR) [20]. These data are complemented by molecular dynamics simulations over a range of component ratios. The MD models were validated against the measured diffusion coefficients and the simulation results were further interpreted, to yield insights into structural justifications for the observed behavior.

2. Experimental

Methanesulfonamide (MSA, melting point 85 °C) and dimethylmethanesulfonamide (DMMSA, melting point 49 °C) (Figure 1) were purchased from Sigma Aldrich (>97%) and dried under vacuum before handling in an argon-filled glove box. Electrochemical grade lithium bis(trifluoromethanesulfonyl)imide (LiTFSI, melting point 235 °C) also obtained from Sigma Aldrich (99.95%). ^{1}H NMR of the resultant deep eutectic electrolyte mixtures did not reveal any water within the NMR detection limit of ~1000 ppm.

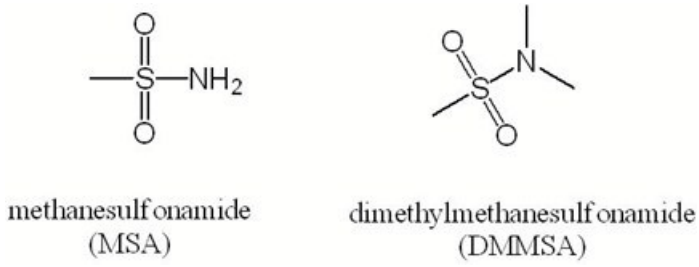

Figure 1: Structural formulae of the organic components considered in this work, methanesulfonamide (MSA) and dimethylmethanesulfonamide (DMMSA)

The diffusion coefficients of the Li^{+} cation, $TFSI^{-}$ anion, and neutral component (MSA or DMMSA) were studied independently, by monitoring the motion of the ^{7}Li, ^{19}F, and ^{1}H nuclei, respectively, by pulsed field gradient NMR (a.k.a. PGFG NMR). The diffusion measurements were conducted as a function of temperature with a Bruker AV300HD

instrument equipped with a Diff50 diffusion probe. Given a maximum gradient strength of ~2,700 G/cm, it was possible to measure diffusion coefficients as small as 10^{-14} m^2/s. Samples were prepared, loaded, and sealed into 5 mm NMR tubes inside of a glove box and subsequently measured over the 25 - 80 °C temperature range, to determine the ^{7}Li (116.642 MHz) and ^{19}F (282.404 MHz) diffusion coefficients. All ^{1}H (300.130 MHz) spectra were collected at temperatures lower than 60 °C, due to physical limitations related to the coil materials. A pulsed field gradient pulse sequence with the inclusion of longitudinal eddy current delays was utilized as previously described by Byrd et al. [21]. This sequence was considered most suitable for this work since it only contains two gradient pulses and two spoiler gradients. This was beneficial, as the relatively short relaxation time T_2^* (≈ 5 ms) observed in the present case can sometimes significantly reduce the S/N ratio if long and/or numerous gradient pulses are used. In addition, the pulse sequence still incorporates eddy current delays which are necessary for samples with a high salt concentration, as in the present case.

Pulses were calibrated to 90° with 9 μs pulses at 40 W, with 4096 points in the time domain, 1 s duration relaxation delay, and 50 ms eddy current delay. Each measurement was temperature-calibrated using an external NMR shift reference. Prior to measurements, ≈20 minutes of temperature equilibration were applied via the use of an appropriate number of dummy scans. Measurements consisted of 8 to 64 scans per gradient increment over a total of 32 increments. The specific number of scans was adjusted in order to achieve a similar S/N ratio for the mixture at all temperatures. The absolute value of the maximum gradient strength was also varied as a function of temperature, in order to enable a measuring range of 5 to 95% for total signal attenuation. This was necessary for achieving optimal sensitivity to the changes in the observed diffusion coefficient. Both gradient pulses were kept at a 2 ms duration, whereas the two spoiler gradients were limited to 1 ms using a diffusion delay which varied from 10 to 50 ms as needed for achieving full resolution of the decay curve. Data processing was performed through the Bruker Topspin 3.2 software using the T_1/T_2 relaxation module. In particular, this involved fitting the attenuation in peak area for the signal of interest. The decay was then fit to an exponential function using known values of the gradient pulse strength, duration, as well as diffusion delay. The resultant fit provided diffusion coefficient values for the nucleus being monitored at a given temperature.

3. Molecular Dynamics Simulations

Initial molecular dynamics simulation parameters involved a total of 500 molecules placed in random spatial positions and orientations using the Packmol software [22]. Simultaneously, an initial set of molecular topologies from the OPLS-AA force field were developed using the MKTOP automatic routine [23]. These topologies were then furthered modified using parameters from the modified OPLSA-AA force field of Lopes et al. [24]. All partial charges were scaled by a factor necessary to reproduce NMR measured diffusion coefficients, typically 85% of their initially calculated values (0.85c). It is important to note however that, while charge scaling performs reasonably well in reproducing the experimentally observed dynamics, there may exist concerns regarding the validity of the overall structure. [25]. A comparison between the computed density and experimental data served as an independent check of the validity of the charge scaling procedure in our study and yielded a discrepancy of ~5%, which should alleviate such concerns. Nevertheless, the effects of charge scaling combined with finite-size effects [26] must always be carefully considered when evaluating results from MD simulations. The MD simulations were performed with the GROMACS 4.62 software package. [27] All simulations were conducted with periodic boundary conditions, with each initial simulation including an energy minimization step through a steepest descent method. This was followed by several isobaric-isothermal (NPT) ensemble simulated annealing steps from the desired temperature (e.g., 298 K) to 600 K over a period of 4 ns, followed by a 2 ns equilibration time at the desired temperature. This was performed in order to reach an equilibrium starting configuration at each desired temperature. The higher temperatures helped in overcoming the slow dynamics of the system and reduced the amount of time required for equilibration. Final runs were conducted in a canonical (NVT) ensemble at the desired temperature over a duration of 30 ns, with 1 ps time steps. Analysis of the simulations was performed through use of select radial distribution functions visualized through the VMD software program.

4. Results and Discussion

Initial performance characterization of deep binary eutectic electrolytes of LiTFSI with MSA and DMMSA was conducted by Halalay et. al., who measured their density and transport properties (dynamic viscosity and specific conductivity) as functions of temperature and

composition [28]. The room temperature ionic conductivity of DMMSA/LiTFSI eutectic mixtures of ~1 mS/cm, while not high enough for use in commercial Li-ion batteries, provides sufficient justification for a more detailed investigation, which is the subject of the present work. The previously measured DEE properties served as parameters for validating the molecular dynamics simulations.

4.1 PFG-NMR Results

Figure 1 displays Arrhenius plots for the temperature dependence of the cation, anion, and neutral component diffusion coefficients at three DMMSA:LiTFSI compositions. An identical analysis performed for MSA:LiTFSI mixtures at the same solvent-to-salt mole ratios is shown in Figure 2.

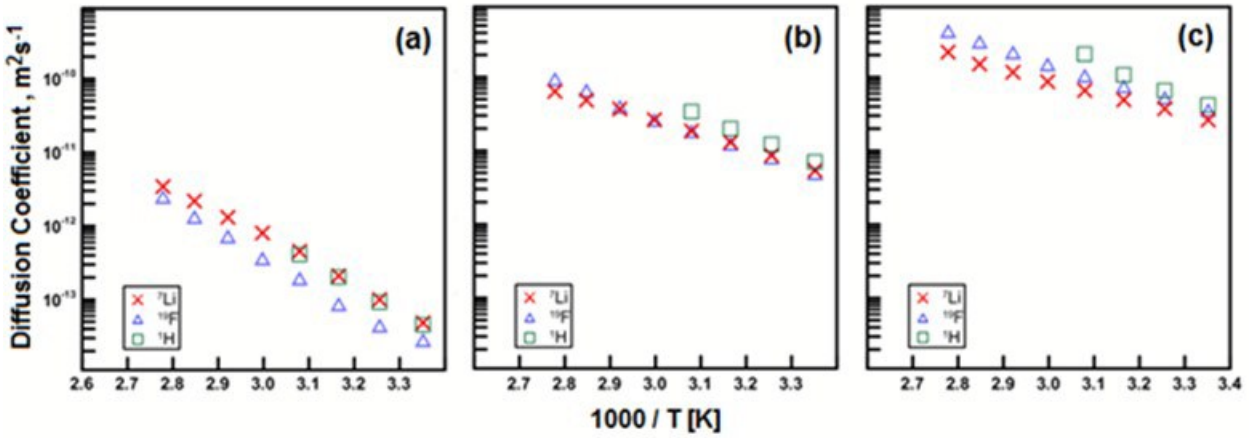

Figure 2: Temperature dependence of the ^{1}H, ^{7}Li, and ^{19}F diffusion coefficients in DMMSA:LiTFSI mixtures at (a) 1:1, (b) 3:1, and (c) 6:1 molar ratios, determined by PFG-NMR.

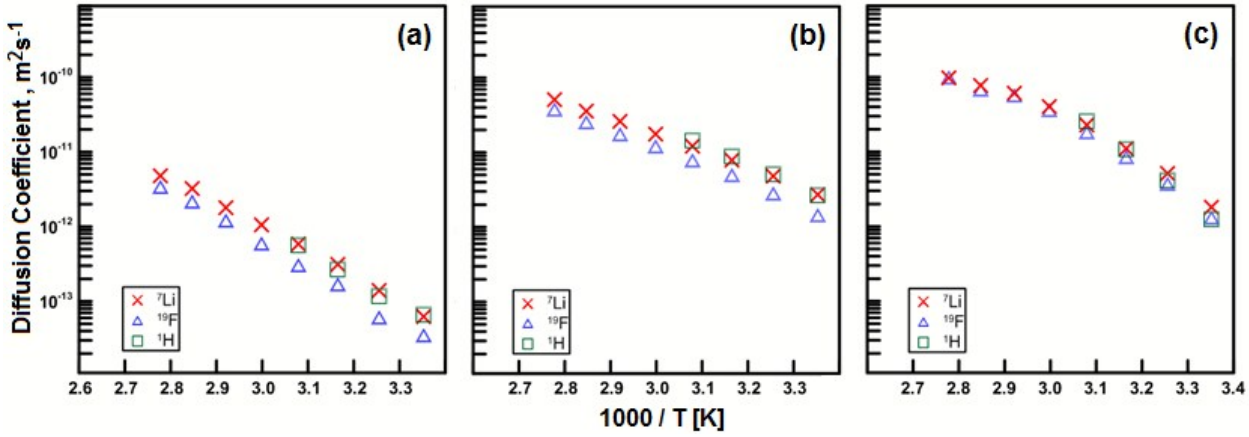

Figure 3. Temperature dependence of the ^{1}H, ^{7}Li, and ^{19}F diffusion coefficients at 1:1 (a), 3:1 (b) and 6:1 (c) MSA:LiTFSI molar ratios, determined through PFG-NMR.

All diffusion coefficients increase monotonically with temperature over the temperature interval investigated in the present study. A monotonic increase in diffusion coefficients with DMMSA content is evident at all temperatures (Fig. 1).In contrast, for MSA-based DEEs all diffusion coefficients increase at high temperatures and exhibit a non-monotonic behavior at the lowest two temperatures when the solvent-to-salt mole ratio changes from 1:1 to 3:1 to 6:1 (Fig. 2).

At 298 K the ^{7}Li diffusion coefficients are 4.8 x 10^{-14}, 5.4 x 10^{-12}, and 2.6 x 10^{-11} m^2/s respectively for 1:1, 3:1, and 6:1 DMMSA:LiTFSI mole ratios. Note that these Li^+ diffusion coefficients are lower by an order of magnitude than values typical for organic solvent:LiTFSI electrolytes. [29] The ^{19}F diffusion coefficients are smaller than those for ^{7}Li, but their relative differences decrease as the temperature increases toward 353 K. A similar trend was observed for the ^{1}H diffusion coefficients. These results correlate well with the decrease in lattice energy associated with the weakening of both Coulombic interactions in LiTFSI and the van der Waals forces between DMMSA molecules. The general trend indicates that an increase in the proportion of the solvent significantly increases the diffusion coefficients of all species. However, there exists a preferential increase in the mobility of both $TFSI^-$ anions and DMMSA molecules relative to Li^+ cations. (Note also that increasing the DMMSA:LiTFSI ratio beyond 6:1 results in the development of regions where recrystallization of DMMSA can be readily observed by visual inspection.)

The ^{7}Li diffusion coefficients for MSA-based DEEs are lower than the corresponding DMMSA-based mixtures, especially at near-ambient temperatures. At 298 K, the ^{7}Li diffusion coefficients are 6.2 x 10^{-14}, 2.7 x 10^{-12} and 1.8 x 10^{-12} m^2/s for 1:1, 3:1, and 6:1 MSA:LiTFSI ratios, respectively. In contrast to DMMSA, the 6:1 MSA:LiTFSI composition exhibits a reduced diffusion coefficient at room temperature relative to the 3:1 composition. The high temperature behavior is more akin to that observed for the DMMSA-based DEEs. The ^{19}F diffusion coefficients become approximately half of those observed for ^{7}Li at the 1:1 and 3:1 compositions, and exhibit a moderate relative increase at the 6:1 composition. These trends were observed at all investigated temperatures. At 298 K, ^{1}H diffusion coefficients have

values very similar to those for ^{7}Li for the 1:1 and 3:1 compositions, with a modest decrease observed at the 6:1 mole ratio. At elevated temperatures, the decrease in ^{1}H diffusion coefficient relative to that of ^{7}Li becomes less pronounced.

For MSA-based DEEs the trends differ somewhat from those for the DMMSA-based DEEs at near-ambient temperatures and with increasing solvent-to-salt ratio. Specifically, comparison of the diffusion coefficients at 298K for the 3:1 and 6:1 MSA:LiTFSI molar ratios shows values which are lower at 6:1 than at 3:1. However, as the temperature increases, the diffusion coefficients quickly achieve and then surpass the values measured at the 3:1 composition. A possible explanation of the observed differences in behavior may result from the substitution of one dialkylamine in DMMSA by one amine functional group in MSA. This configuration gives MSA an increased hydrogen bonding capacity, which is the likely cause for the observed change in behavior. The hydrogen bonding capacity can directly influence the diffusion of MSA molecules and $TFSI^{-}$ anions, since both can form hydrogen bonds which hinder diffusion. However, this dynamical limitation is overcome at higher temperatures, because of the directional nature and relatively the low strength of the hydrogen bonds. Ultimately this yields the deviation from linearity, i.e., deviation from Arrhenius behavior, of the diffusion coefficient as a function of temperature at 6:1 MSA:LiTFSI as compared to the 3:1 composition.

It is useful to examine how the diffusivity and conductivity of the DEEs considered here compare with electrolyte solutions based on organic solvents or ionic liquids with LiTFSI as the lithium salt. This is particularly important, given the roles that the relative values of diffusivity and transport properties play in determining the overall LIB performance. From a comparison of the Hayamizu et al. results determining the diffusion coefficients of fourteen LiTFSI solutions in organic solvents [29], it is immediately apparent is that ^{7}Li diffusivities in organic liquids are more than an order of magnitude higher than those for the DEEs examined in the present work. However, the respective ionic conductivities vary considerably less, by factors ranging from 3 to 8 [28]. The observed differences stem from a variety of factors, including the relative ease of dissociating LiTFSI, and that the DEEs contain larger concentrations of Li salt compared with LiTFSI solutions in aprotic organic solvents. Therefore, the handicap of a considerably slower Li^{+} dynamics in the deep eutectic electrolytes compared with liquid electrolyte solutions is made up to some extent by the

increased lithium salt concentration in the former.

In contrast to organic solvents, ILs display similarly low diffusivities as do DEEs, although this is due to the high electrostatic (a.k.a. Coulombic) interaction energies. While modifications to the anion or cation geometry are often performed in order to weaken Coulombic interactions, they nevertheless remain the limiting factor. (For comparison , note that the diffusion coefficient of lithium in the ternary [$emim^+$][$TFSI^-$][Li^+] ionic liquid is approximately 10^{-11} m^2/s at 298 K [30]. Also note that, while the specific conductivity of this IL is several times higher than that the values reported for the DEEs from the present work, a significant fraction of this conductivity is not due to Li^+ cations, as indicated by its extremely low Li^+ transport number (≈ 0.02). (While transference numbers and transport numbers do not have – in the strictest sense – identical meanings, since they are ratios of physical quantities with different dimensions [31], they differ by less than 5% in most cases of interest. They can therefore be used interchangeably to some extent, especially when encountering large differences between these ratios during materials comparisons, as in the present case.) A low Li^+ transport number leads to the development of detrimental concentration gradients, particularly at high current densities. In contrast, the transport numbers for the DEEs investigated in the present work is (shown as a function of temperature in Figure 3) have considerably larger values, ranging from 0.40 to 0.70 for DMMSA:LiTFSI and from 0.55 to 0.70 for MSA:LiTFSI at temperatures of interest for the LIBs operation.

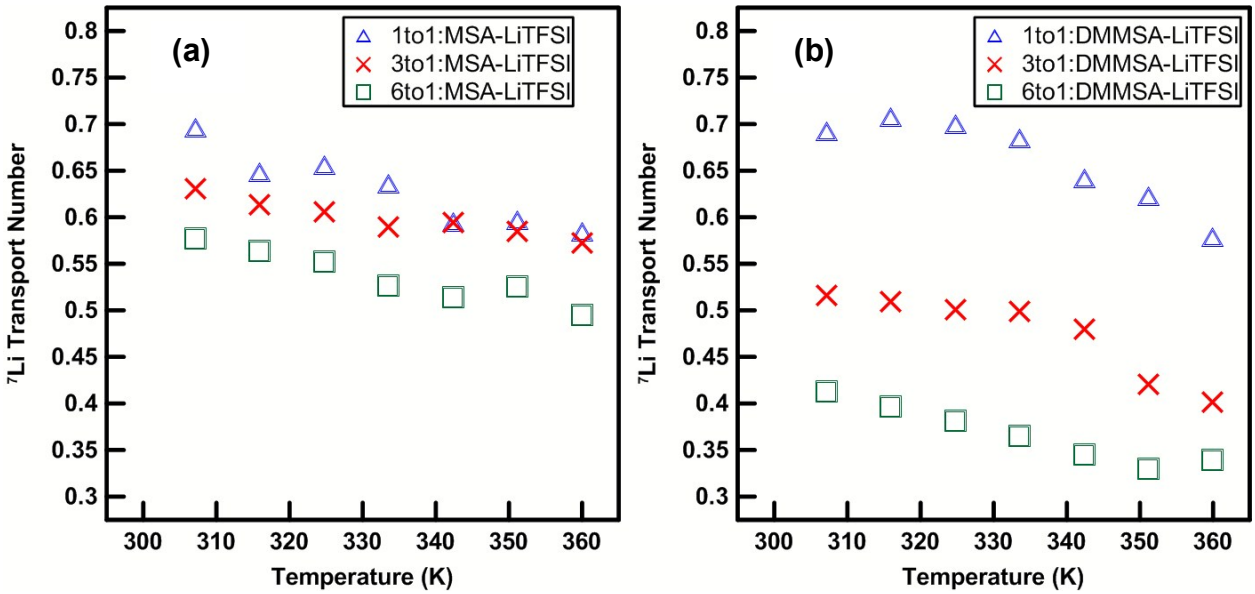

Figure 4: Variation of the lithium transport numbers with temperature derived from ^{1}H, ^{7}Li, and ^{19}F diffusion coefficient measurements for 1:1, 3:1 and 6:1 mole ratios of MSA:LiTFSI (a) and DMMSA:LiTFSI (b).

Immediately apparent are the high lithium transport numbers at the 1:1 compositions, with values near 0.7 at room temperature, which are significantly higher than the 0.25 to 0.4 values typical for organic carbonate based electrolytes [32]. Decreasing trends in the lithium transport number were obtained both as a function of temperature and solvent-to-salt mole ratio. It is noteworthy that for the MSA-based DEEs the transport numbers exceed 0.5 even for the dilute solution, and for DMMSA-based DEEs transport numbers similar to those of state-of-the-art liquid electrolyte solutions are obtained for the dilute (6:1 mole ratio) solution. Thus the transport numbers for these DEEs are at least 25x greater than those for the $[EMIM^{+}][TFSI^{-}][Li^{+}]$ ionic liquids. Therefore, despite a lower ionic conductivity, they may enable LIB performance, provided they exhibit electrochemical stability windows which accommodate electrode materials typical for LIBs and also have favorable film-forming properties.

One rationalization of the observed transport number behavior comes from a consideration of the lithium coordination environment. The high positive charge density of the Li^{+} cations tends to center the coordination environment on it. Therefore one must consider three kinds of diffusion: independent movement of Li^{+} cations from one coordination environment to another, concerted diffusion of Li^{+} together with its coordination environment, and independent movement of the coordination environment components. If all components diffuse as at the same rate, transport numbers of 0.5 will result for both cations and anions. Deviations from 0.5 can only result from the faster diffusion of one species relative to the others. When the viscosity is high, the energy barrier to independent movement for a large molecule such as $TFSI^{-}$ is greater than that for unsolvated Li^{+}. The limiting case for this situation would be a solid lithium conductor where only Li^{+} is diffusing relative to a stationary anionic matrix. As the viscosity decreases, the energy barrier for independent $TFSI^{-}$ diffusion may become equal to or even smaller than that for the Li^{+} cation. Such behavior must originate from a change in the relative magnitude of the intermolecular forces which limit the diffusion of ions. Further support for this argument is provided by Figure 3, which displays a

decrease in the lithium transport number of DMMSA based DEEs relative to MSA based ones at the two more dilute compositions. The capacity for hydrogen bonding of MSA increases the magnitude of the van der Waals (vdW) interactions, i.e., the dipole-dipole forces. These contribute to the slowing of $TFSI^-$ diffusion to a greater extent than Li^+ diffusion, as the anion is disproportionately affected by van der Waals forces. Unfortunately, the introduction of hydrogen bonding also leads to a slowing of overall diffusion. Nevertheless, its incorporation may increase the lithium transport number by slowing the diffusion of anions.

Furthermore, evaluation of the transport properties with respect to ionicity was conducted. However, the limited access to temperature dependent conductivity data has relegated the data to figure S-5 of the supplementary information. The trend in ionicity mirrors that observed in the lithium transport numbers. However, their overall magnitude appears anomalously low and as such there is still some question about their reliability.

3.2. Molecular Dynamics Simulation Results.

Molecular dynamics (MD) simulations were conducted to obtain further insights into the solution state structure of the deep eutectic electrolytes and thus aid the interpretation of the diffusion data obtained by NMR. The primary method we used for interpreting the results of MD simulations is based on the radial distribution function (RDF) [33], a powerful tool for characterizing the time dependent atomic environment surrounding a chemical species of interest. The RDF is a particularly valuable investigation tool for systems devoid of long-range order such as liquids and glasses.

Figure 4 displays the RDFs of Li^+ cations relative to the nitrogen atoms in $TFSI^-$ (panel a) and MSA (panel b). Three peaks are visible in both cases. The smaller peak at the shortest (~3 Å) distance corresponds to direct lithium-nitrogen coordination. Since nitrogen is a site with negative charge density, direct coordination is possible, though relatively unlikely. However, this interaction is stronger with $TFSI^-$ than with MSA. The two larger peaks at ~4.5, and 5.0 Å distances are the result of the (Coulombically-driven) lithium-oxygen coordination. They specifically correspond to bidentate and monodentate coordination of $TFSI^-$ to Li^+, respectively.

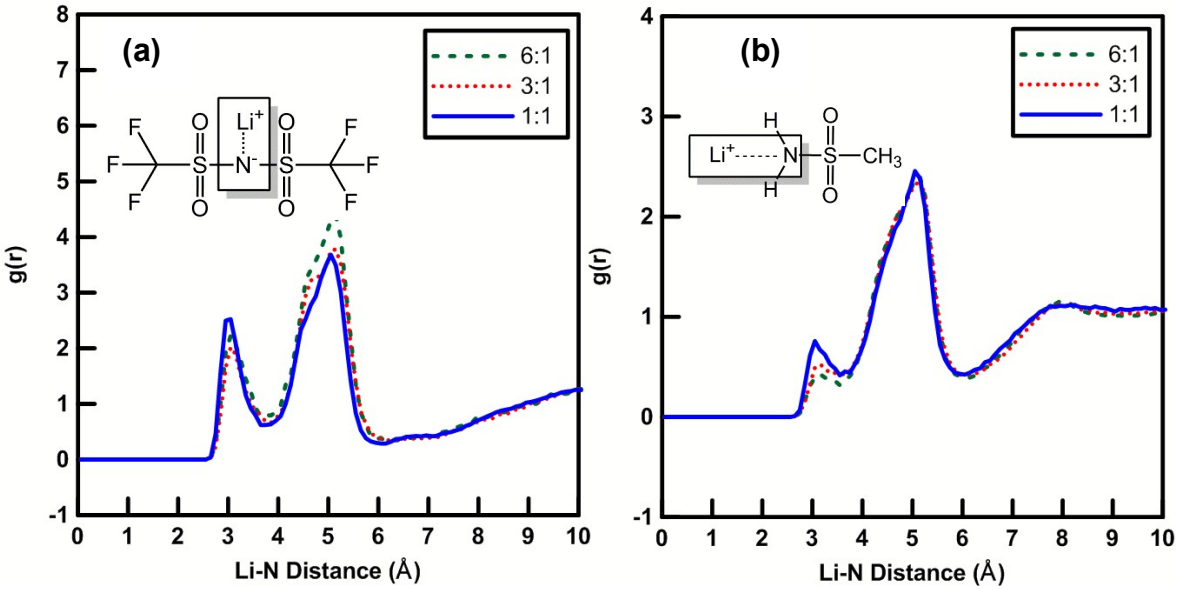

Figure 5: Lithium-nitrogen radial distribution functions for Li^+ contact with $TFSI^-$ (a) and MSA (b) at 298K in MSA:LiTFSI mixtures.

Comparison of this data with the RDFs for the DMMSA:LiTFSI system (see Figure 5) indicates no direct coordination of Li^+ cations by nitrogen in DMMSA, but a slightly increased coordination by N in $TFSI^-$ over what is observed for MSA:LiTFSI (Fig. 4). The proportion between the bidentate and monodentate coordinations increases as a function of greater organic content. Though for MSA the effect is substantially smaller than for DMMSA. This is a consequence of MSA being better able to compete for lithium coordination than DMMSA. Also, the greater favourability of the $TFSI^-$ to Li^+ contacts with DMMSA is further exemplified by the increasing proportion of bidentate to monodentate coordination.

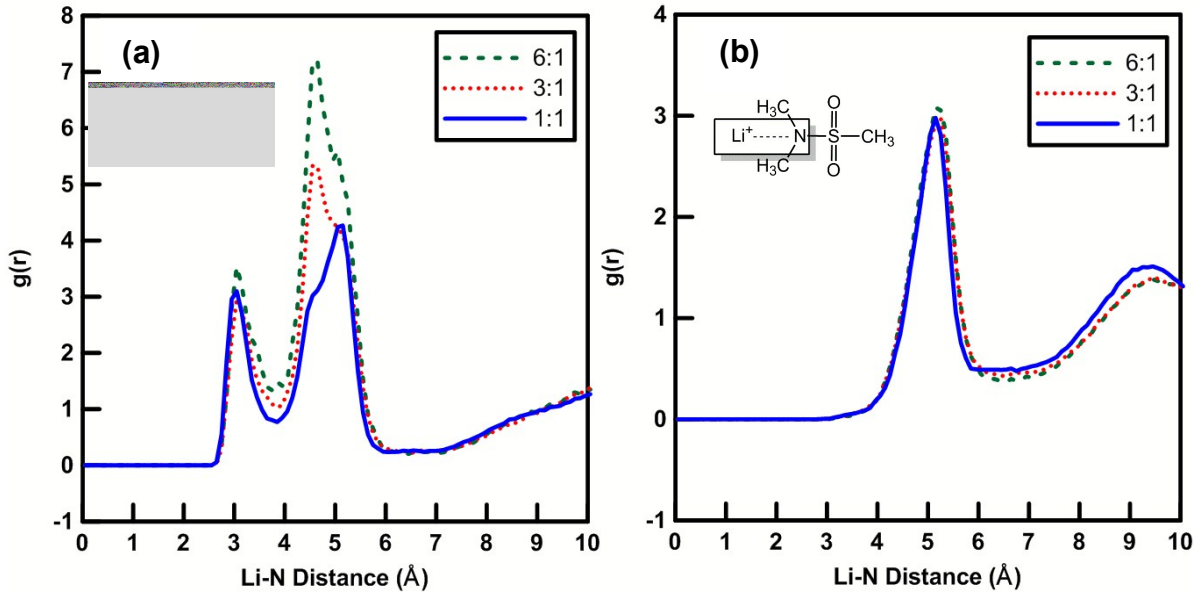

Figure 6: Lithium-nitrogen radial distribution functions for intermolecular between contact between Li^+ and $TFSI^-$ (a) or DMMSA (b) at 298 K in DMMSA:LiTFSI mixtures.

Comparison of Figures 6 and 7 reveals some important features of the lithium coordination environment with regard to direct lithium-oxygen contacts. Foremost are the amplitudes of the RDFs at 3 Å being well above that in the RFD values for the Li^+ cation coordination by nitrogen at the same (nearest-neighbor) distance. This indicates a strong correlation between the presence of lithium and oxygen at this distance, suggesting that these are the strongest intermolecular interactions in the system. Referring to Figure 6 in particular, the small differences in the RDFs for $TFSI^-$ and MSA shows that the differences in their coordination of Li^+ are surprisingly small. This indicates that, despite its neutral charge profile, MSA competes quite effectively for lithium coordination and is a key factor for the deep eutectic formation, since it is the competition for the lithium cation which breaks the ionic bonds in the LiTFSI salt.

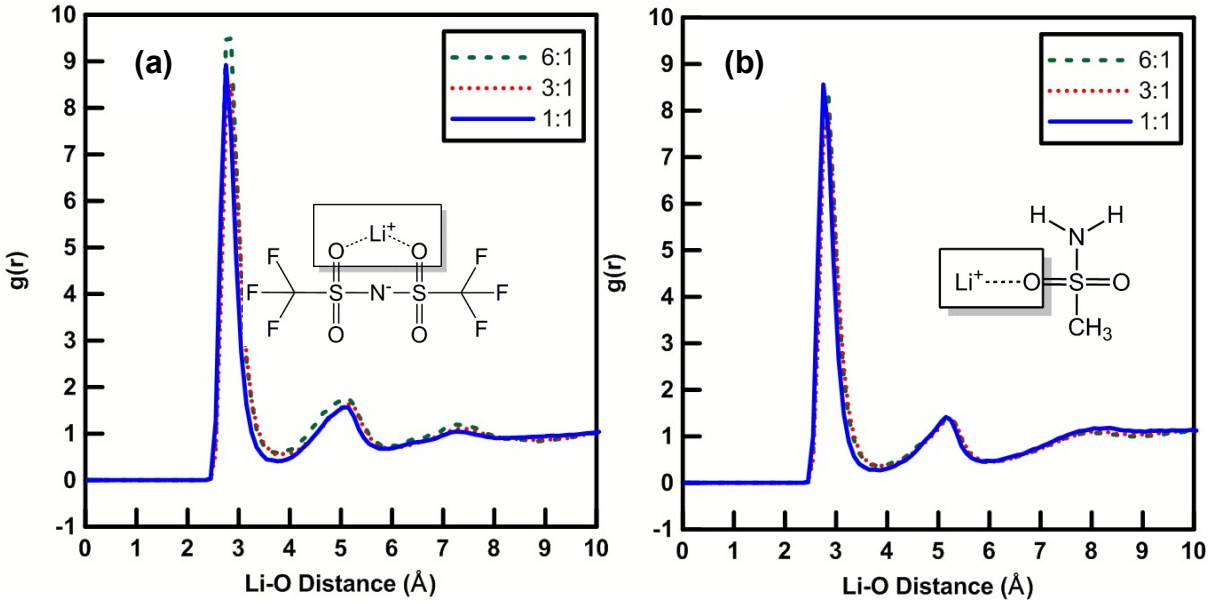

Figure 7: Lithium – oxygen radial distribution functions for intermolecular contact between Li^+ and $TFSI^-$ (a) or MSA (b) at 298 K for MSA:LiTFSI mixtures.

MSA-based Li^+-O contacts display no substantial changes in the RDFs with changing MSA content in the DEE. This is, however, not the case for DMMSA (Figure 7) where the RDF associated with the Li^+ coordination by the O atoms in $TFSI^-$ displays a significant increase with DMMSA content, whereas the coordination of Li^+ by the O atoms in DMMSA does not change. This discrepancy can be attributed to the preferential association of Li^+ with $TFSI^-$ over DMMSA. Since the DMMSA molecule does not have any easily accessible sites with significant positive charge density, it cannot compete with Li^+ for coordinating $TFSI^-$ and hence there is an increase in the density of $TFSI^-$ in the vicinity of Li^+ cations. This contrasts with MSA, where the positively charged hydrogen in the amine functional group competes successfully with Li^+ for oxygen coordination. The result is increased competition for $TFSI^-$ by MSA, which competitively reduces the extent of TFSI- coordination with lithium.

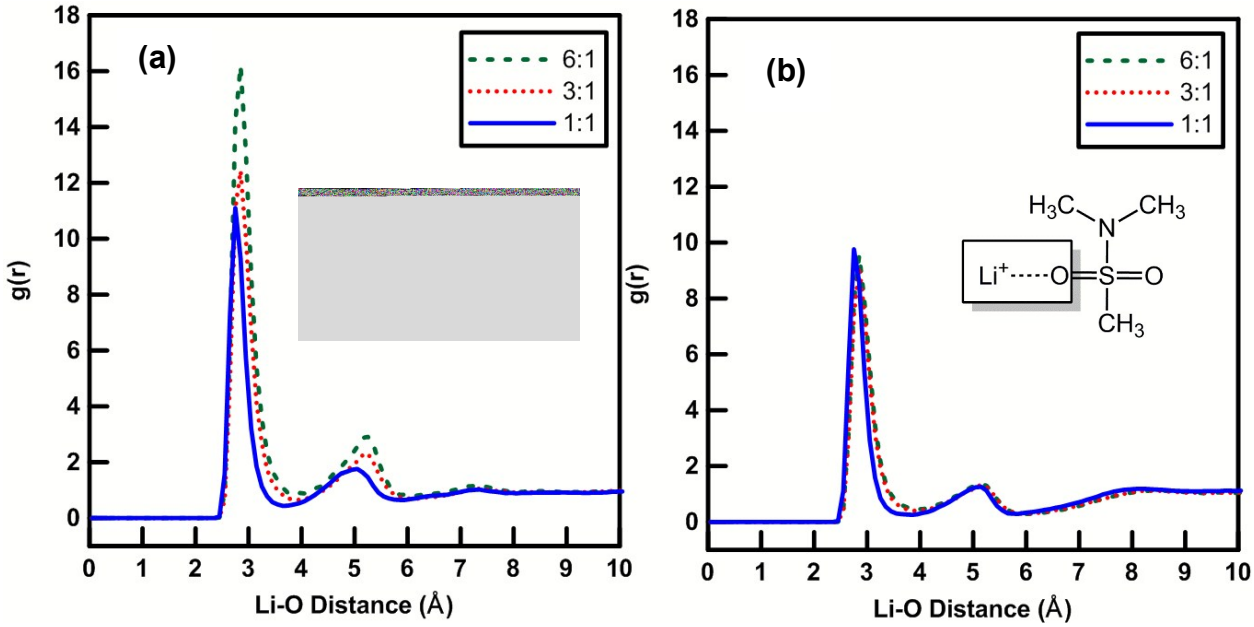

Figure 8: Lithium – oxygen radial distribution functions for intermolecular contact between Li^+ cations and $TFSI^-$ (a) or DMMSA (b) in DMMSA:LiTFSI at 298 K.

Since the extent of hydrogen bonding appears to have such a significant impact on DEEs properties, we determined and then examined the RDFs for oxygen-hydrogen contacts. Figure 8 confirms the existence of hydrogen bonding via the intermolecular peak that appears at ~1.8 Å. As expected, hydrogen bonding exists between MSA molecules as well as between MSA and $TFSI^-$. Additionally, the intensity of the peak corresponding to the hydrogen bond increases with MSA content, consistent with the increase in sites available for hydrogen bonding.

An interesting temperature dependence was observed for hydrogen bonding interactions, which is illustrated with Figures 8 and 9. The extent of hydrogen bonding was observed to diminish, as revealed by a significant decrease in intensity, well beyond that observed for any other atom pair. This observation is consistent with an increase in the diffusion coefficients with temperature shown in Figure 1, which can now be attributed to the weakening of the hydrogen bonding network. As a point of comparison, Figures 10 and 11 indicate the absence of the hydrogen bonding peak in DMMSA:LiTFSI mixtures, which is to be expected because DMMSA is incapable of participating in hydrogen bonding. This further confirms the trends observed in Figure 1 (b) and (c), where the diffusion coefficients of all

species in DMMSA:LITFSI at low temperatures are considerably higher than the values observed for the same diffusion coefficients in MSA:LiTFSI, as shown in Figure 1 (b) and (c).

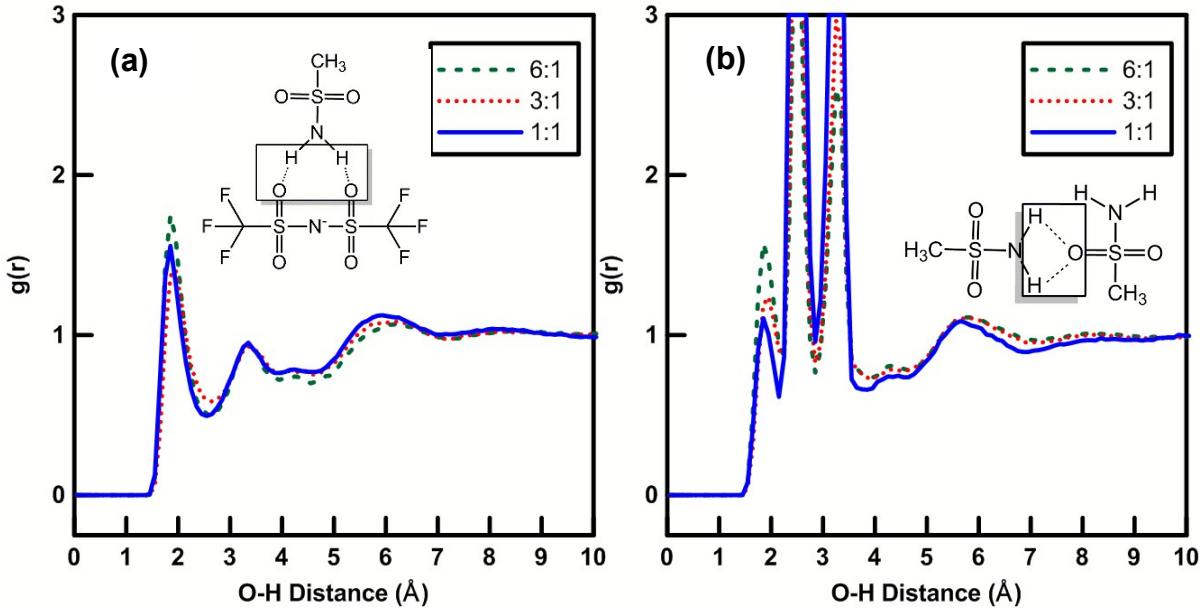

Figure 9: Oxygen – hydrogen radial distribution functions for intermolecular contact between MSA and $TFSI^-$ (a) or MSA (b) in MSA:LiTFSI mixtures at 298 K.

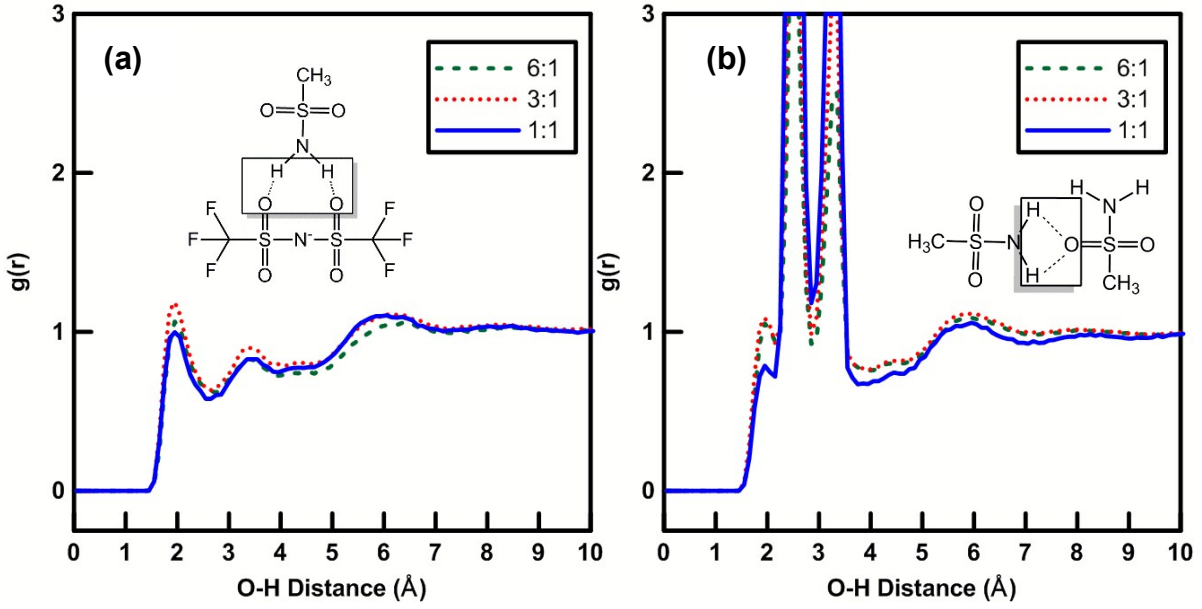

Figure 10: Oxygen – hydrogen radial distribution functions for intermolecular contact between MSA and $TFSI^-$ (a) or MSA (b) in MSA:LiTFSI mixtures at 358 K.

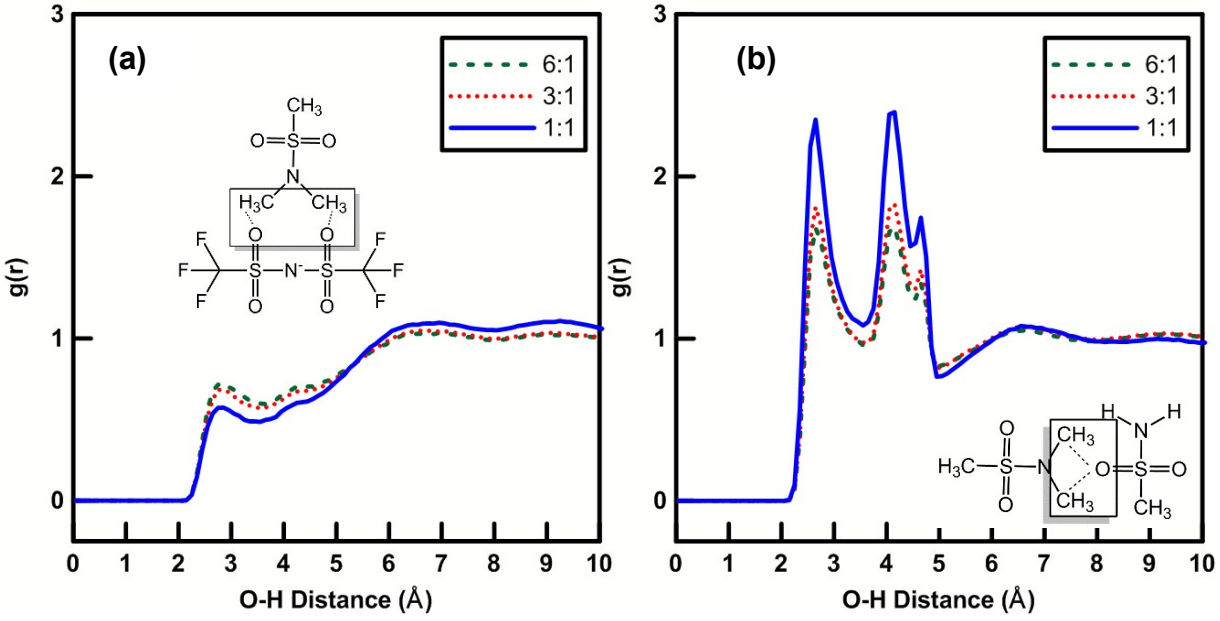

Figure 11: Oxygen – hydrogen radial distribution functions for intermolecular contact between DMMSA and $TFSI^-$ (a) or DMMSA (b) in DMMSA:LiTFSI mixtures at 298 K.

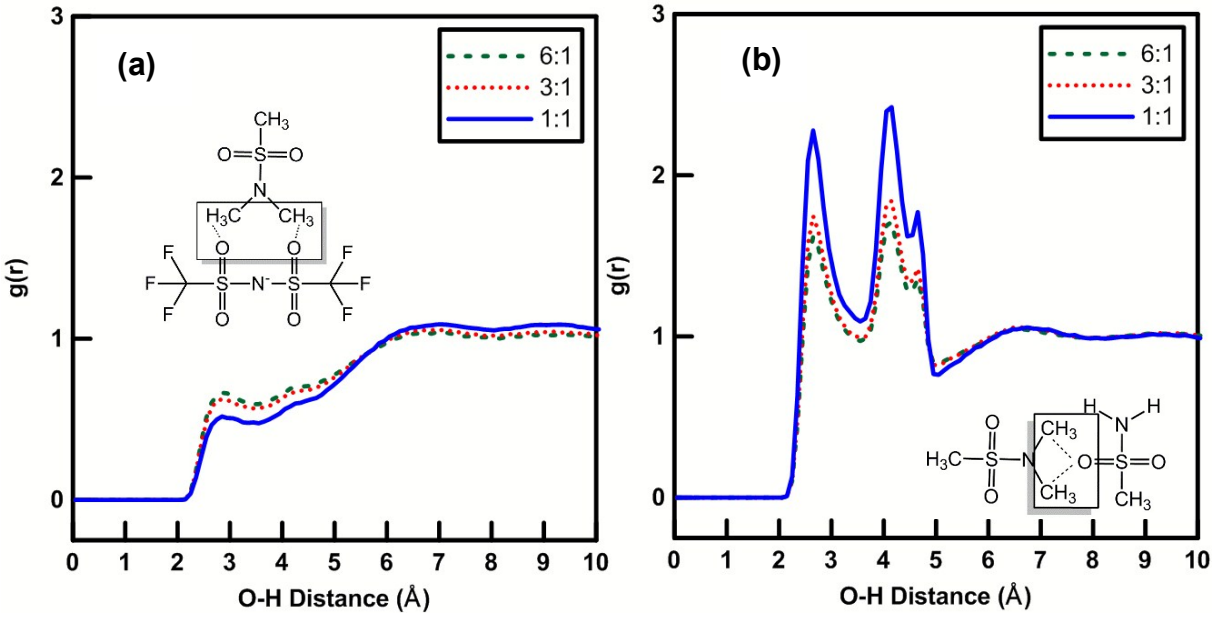

Figure 12: Oxygen – hydrogen radial distribution functions for intermolecular contacts between DMMSA and $TFSI^-$ (a) or DMMSA (b) in DMMSA:LiTFSI mixtures at 358 K.

4. Conclusions

Sulfonamide-based deep eutectic electrolytes (DEEs) were previously shown to have lithium conductivities within less than a factor of 3 from traditional $LiPF_6$/carbonates electrolytes. The PFG NMR measurements reported here indicate that the lithium transport number varies significantly with DEEs composition. Its magnitude was found to be at least the same as, and often significantly higher, than transport numbers of state-of-the-art ($LiPF_6$/mixed organic carbonates) LIB electrolytes, i.e., in the 0.40 to 0.71 range. Reasons for this behavior were proposed using a combination of the NMR experiments and MD simulations.

The systems studied here are dominated by interactions between the Li^+ cation and oxygen from both the anion and the organic component. It is this competitive feature which allows the eutectic formation. However, fine-tuning of the fluid and diffusion properties depends very significantly on van der Waals interactions. Dipole-dipole attractive interactions, while hindering overall diffusion, can nevertheless enhance the lithium transport number by slowing the translational motion of the $TFSI^-$ anions more than that of the Li^+ cations. In principle, any molecule with a significant amount of accessible positive charge density could influence the anion in a similar manner and therefore increase the Li^+ transport (or transference) number, although at a possible decrease in overall diffusivity.

Deep eutectic electrolytes represent a relatively unexplored class of electrolytes that are promising from both cost and practical utility perspectives. While DEEs based on hydrogen bonding are the most common, as they often correspond to molecules with large dipole moments, the latter is not a prerequisite for the formation of eutectics. Significant room for further research into this topic is still available through an expansion of the sample space, in the search for formulations with improved properties from a practical point of view (i.e., increased specific conductivity over a broad temperature range, improved transference numbers over those typical for $LiPF_6$/carbonates, oxidation potentials exceeding 5 V vs. Li/Li^+).

Electronic Supplementary Information: Figures S-1 thorough S-4 display the volume integrals $G(R)$, for the lithium- nitrogen (Figs. S-1 and S-2) and lithium-oxygen interactions. They provide further detail to the discussion of the coordination environments surrounding the lithium cations. Supplementary Information is available free of charge at (www.rsc.org/pccp)

Acknowledgements

The authors gratefully acknowledge funding through the NSERC APC program and by GM of Canada. They also thank Dr. Bob Powell for carefully reviewing the manuscript and for excellent editorial suggestions.

References

[1] Lewandowski, A. Ionic liquids as electrolytes for Li-ion batteries - An overview of electrochemical studies. *J. Power Sources* **194** (2009) 601–609.

[2] Zhang, S.; Sun, N.; He, X.; Lu, X.; Zhang, X. Physical properties of ionic liquids: database and evaluation. *J. Phys. and Chem. Ref. Data* **35** (2006) 1475.

[3] Hayyan, M.; Mjalli, F. S.; Hashim, M. A.; Al Nashef, I. M.; Mei, T. X. Investigating the electrochemical windows of ionic liquids. *J. Ind. Eng. Chem.* **19** (2013) 106–112.

[4] Krachkovskiy, S. A.; Pauric, A. D.; Halalay, I. C.; Goward, G. R. Slice-selective NMR diffusion measurements: a robust and reliable tool for in situ characterization of ion-transport properties in lithium-ion battery electrolytes. *J. Phys. Chem. Lett.* **4** (2013) 3940–3944.

[5] Zhang, Q.; Vigier, K. D. O.; Royer, S.; Jérôme, F. Deep eutectic solvents: syntheses, properties and applications. *Chem. Soc. Rev.* **41** (2012) 7108–7146.

[6] Abbott, A. P.; Boothby, D.; Capper, G.; Davies, D. L.; Rasheed, R. K. Deep eutectic solvents formed between choline chloride and carboxylic acids: versatile alternatives to ionic liquids. *J. Am. Chem. Soc.* **126** (2004) 9142–9147.

[7] Sun, H.; Li, Y.; Wu, X.; Li, G. Theoretical study on the structures and properties of mixtures of urea and choline chloride. *J. Mol. Model.* **19** (2013) 2433–2441.

[8] Pandey, A.; Rai, R.; Pal, M.; Pandey, S. How polar are choline chloride-based deep eutectic solvents? *Phys. Chem. Chem. Phys.* **16** (2013) 1559–1568.

[9] Ueno, K.; Yoshida, K.; Tsuchiya, M.; Tachikawa, N.; Dokko, K.; Watanabe, M. Glyme−Lithium Salt Equimolar Molten Mixtures: Concentrated Solutions or Solvate Ionic

Liquids? *J. Phys. Chem. B* **116** (2012) 11323−11331.

[10] Frömling, T.; Kunze, M.; Schönhoff, M.; Sundermeyer, J.; Roling, B. Enhanced Lithium Transference Numbers in Ionic Liquid Electrolytes. *J. Phys. Chem. B* **2008**, *112* (41), 12985–12990.

[11] Zugmann, S.; Fleischmann, M.; Amereller, M.; Gschwind, R. M.; Wiemhöfer, H. D.; Gores, H. J. Measurement of Transference Numbers for Lithium Ion Electrolytes via Four Different Methods, a Comparative Study. *Electrochimica Acta* **2011**, *56* (11), 3926–3933.

[12] Liang, H.; Li, H.; Wang, Z.; Wu, F.; Chen, L.; Huang, X. New binary room-temperature molten salt electrolyte based on urea and LiTFSI. *J. Phys. Chem. B* **105** (2001) 9966–9969.

[13] Hu, Y.; Li, H.; Huang, X.; Chen, L. Novel room temperature molten salt electrolyte based on LiTFSI and acetamide for lithium batteries. *Electrochemistry Communications* **6** (2004) 28–32.

[14] Chen, R.; Wu, F.; Liang, H.; Li, L.; Xu, B. Novel binary room-temperature complex electrolytes based on LiTFSI and organic compounds with acylamino group. *J. Electrochem. Soc.* **152** (2005) A1979–A1984.

[15] Boisset, A.; Menne, S.; Jacquemin, J.; Balducci, A.; Anouti, M. Deep eutectic solvents based on N-methylacetamide and a lithium salt as suitable electrolytes for lithium-ion batteries. *Phys. Chem. Chem. Phys.* **15** (2013) 20054–20063.

[16] Menne, S.; Pires, J.; Anouti, M.; Balducci, A. Protic ionic liquids as electrolytes for lithium-ion batteries. *Electrochemistry Communications* **31** (2013) 39–41.

[17] Fehrmann, R.; Riisager, A.; Haumann, M. *Supported Ionic Liquids: Fundamentals and Applications*; John Wiley & Sons, New York, 2013.

[18] Israelachvili, J. N.; Tabor, D. The measurement of van der Waals dispersion forces in the range 1.5 to 130 Nm. *Proc. Royal Soc. London A* **331** (1972)19–38.

[19] Tang, B. Recent developments in deep eutectic solvents in chemical sciences. *Monatshefte Chem.* **144** (2013) 1427–1454.

[20] Stejskal, E. O.; Tanner, J. E. Spin diffusion measurements: spin echoes in the presence of a time-dependent field gradient. *J. Chem. Phys.* **42** (1965) 288–292.

[21] Altieri, A. S.; Hinton, D. P.; Byrd, R. A. Association of biomolecular systems via pulsed field gradient NMR self-diffusion measurements. *J. Am. Chem. Soc.* **117** (1995) 7566–7567.

[22] Martínez, L.; Andrade, R.; Birgin, E. G.; Martínez, J. M. PACKMOL: A package for building initial ocnfigurations for molecular dynamics simulations. *J. Comput. Chem.* **30** (2009) 2157–2164.

[23] Ribeiro, A. A. S. T.; Horta, B. A. C.; Alencastro, R. B. de. MKTOP: a program for automatic construction of molecular topologies. *J. Brazilian Chem. Soc.* ***19*** (2008) 1433–1435.

[24] Canongia Lopes, J. N.; Deschamps, J.; Pádua, A. A. H. Modeling ionic liquids using a systematic all-atom force field. *J. Phys. Chem. B* **108** (2004) 2038–2047.

[25] Schröder, C. Comparing Reduced Partial Charge Models with Polarizable Simulations of Ionic Liquids. *Phys. Chem. Chem. Phys.* **2012**, *14* (9), 3089–3102.

[26] Baumketner, A.; Chushak, Y. Correction for Finite-Size Effects in Molecular Dynamics Simulation of Liquid Alloys. *J. Non-Cryst. Solids* **1999**, *250–252, Part 1*, 354–359.

[27] Van Der Spoel, D.; Lindahl, E.; Hess, B.; Groenhof, G.; Mark, A. E.; Berendsen, H. J. C. GROMACS: fast, flexible, and free. *J. Comput. Chem.* **26** (2005)1701–1718

[28] Geiculescu, O. E.; Des Marteau, D. D.; Creager, S. E.; Haik, O.; D. Hirshberg, D.; Shilina, Y.; Zinigrad, E.; Levi, M.D.; Aurbach, D; and Halalay, I. C.; Binary deep eutectic electrolytes for rechargeable Li-ion batteries based on mixtures of sulfonamides and lithium perfluorosulfonimide salts, accepted for publication in *J. Power Sources* (2016).

[29] Hayamizu, K.; Aihara, Y.; Arai, S.; Garcia. Pulse-Gradient Spin-Echo ^{1}H, ^{7}Li, and ^{19}F NMR diffusion and ionic conductivity measurements of 14 organic electrolytes containing $LiN(SO_2CF_3)_2$. *J. Phys. Chem. B* **103** (1999) 519–524.

[30] Lesch, V.; Jeremias, S.; Moretti, A.; Passerini, S.; Heuer, A.; Borodin, O. A Combined theoretical and experimental study of the Influence of Different anion ratios on lithium ion dynamics in ionic liquids. *J. Phys. Chem. B* **118** (2014) 7367–7375.

[31] Sethurajan, A.K; Krachkovskiy, S.K.; Halalay, I.C.; Goward, G.R.; Protas, B. Accurate Characterization of ion transport properties in electrochemical systems using in-situ NMR imaging and inverse modeling, accepted for publication in *J. Phys. Chem. B*. (2015)

[32] Valøen, L. O.; Reimers, J. N. Transport properties of $LiPF_6$-based Li-ion battery electrolytes. *J. Electrochem. Soc.* **152** (2005) A882–A891.

[33] Keizer, J. *Statistical Thermodynamics of Nonequilibrium Processes*; Springer Science & Business Media, 1987.